SEMARAK ILMU PUBLISHING

Journal of Advanced Research in Applied Sciences and Engineering Technology

Journal homepage:
https://semarakilmu.com.my/journals/index.php/applied_sciences_eng_tech/index
ISSN: 2462-1943

Sustainable Biochar Carbon Biosorbent Based on Tamarind (*Tamarindusindica* L) Seed: Literature Review, Preparation, and Adsorption Isotherm

Asep Bayu Dani Nandiyanto[1,*], Meli Fiandini[1], Risti Ragadhita[1], Hanifa Maulani[1], Muthia Nurbaiti[1], Abdulkareem Sh. Mahdi Al-Obaidi[2], Jumril Yunas[3], Muhammad Roil Bilad[4]

[1] Fakultas Pendidikan Matematika dan Ilmu Pengetahuan Alam, Universitas Pendidikan Indonesia, Jl. Dr. Setiabudhi no. 229, Bandung, 40154, Indonesia
[2] School of Engineering, Taylor's University, Selangor, Malaysia
[3] Institute of Microelectronic and Nanotechnology (IMEN), Universiti Kebangsaan Malaysia, Malaysia
[4] Universiti Brunei Darussalam, Brunei Darussalam

ARTICLE INFO

Article history:
Received 3 April 2023
Received in revised form 22 July 2023
Accepted 18 August 2023
Available online 2 September 2023

Keywords:
Adsorbate loading; Adsorption isotherm; Bioadsorbent; Biochar; Carbon; Curcumin dye; Organic waste; Particle size; Tamarind Seeds

ABSTRACT

In the need for a sustainable environment and clean water for assisting sustainable development goals (SDGs) in developing countries, this study demonstrates the way how to produce biochar carbon microparticles from tamarind seed waste and investigates the proposal mechanism during the adsorption by comparing results with ten adsorption isotherm models. In short, carbon microparticles (sizes of 500, 1000, and 2000 μm) were prepared by carbonizing saw-milled tamarind seeds at 250˚C. The adsorption was evaluated in the batch reactor for adsorbing curcumin (as a model of dye). The models confirmed the formation of a layer with physisorption characteristics and binding energy due to the existence of the Van der Waals force. The adsorption profile was also done by varying adsorbent sizes and initial adsorbate loadings. Small-sized adsorbents gave impacts the improvement of adsorption capacity due to the presence of a larger surface area, a larger number of adsorption sites, and additional adsorbate-adsorbate interaction. Fewer loadings of the adsorbate results in less adsorption efficacy due to the less adsorbate-adsorbent contact and interaction. Understanding the processes happening is beneficial for future advances and applications, such as catalysts and adsorbents, particularly concerning the utilization of carbon materials from organic waste.

1. Introduction

Clean water availability is becoming a popular artist recently [1]. The need for a sustainable environment and clean water for supporting sustainable development goals (SDGs) in developing countries is important. In many nations, the SDGs are increasingly being taught in schools as a goal for education [2, 3]. Water is a necessary resource for the survival of various life, including humans,

* *Corresponding author.*
E-mail address: nandiyanto@upi.edu

https://doi.org/10.37934/araset.32.1.210226

animals, and cattle, as well as the growth of plants, making water scarcity and water pollution to be two major issues recently [4].

To treat wastewater, several techniques have been reported, such as coagulation, nano-filtration, ozonolysis, membrane filtration, oxidation process, and adsorption [4-12]. Because of its simplicity, efficiency, and visibility, adsorption is the most useful technique. The adsorption technique has been investigated as an ideal alternative to other expensive wastewater treatment methods [13]. To support the SDGs, the quest for the use of cheap, readily available, efficient, and environmentally friendly adsorbents is crucial. Biochar or carbon materials are one of the effective materials, making them to be well-research [14-29]. Several adsorbents have been proposed using agricultural waste, from leaves, seeds, roots, and bark [30]. Here based on our previous studies using pineapple peel [31], pumpkin seed [7], rice straw and rice husk [32,33], soursop peel [34], and red dragon fruit peel [35]), this study reported the use of carbon microparticle adsorbent from tamarind (*Tamarindusindica* L) seeds as the main resource. Tamarind has been widely used as a spice mixture in many foods, while its seeds (containing high cellulose) are disposed of directly. Tamarind seed contains 67 g/Kg of crude fiber and a high percentage of carbohydrates, indicating its prospectiveness as a carbon source [36]. Tamarind seeds that are considered solid waste were treated and converted into carbon with no chemical modification.

Although some researchers have reported the use of biosorbent, the use of tamarind seeds has not been reported yet, especially when it is completed with adsorption isotherm analysis. Particle size parameters and adsorbate loadings were investigated to support the precise analysis of the adsorption mechanism. Carbon microparticles (sizes of 500, 1000, and 2000 μm) were contacted with curcumin (as a model of dye) in the batch reactor, and the results were compared to ten adsorption isotherm models to understand the mechanism during the adsorption. Curcumin was used as a model since its size can represent the sizes of commercially available dyes.

2. Biochar Production

To create biochar, biomass is being used. Many papers discussed about the biochar formation [37]. The conversion of biomass into biochar has been growing interest since its uses in various applications. One of the best method is thermochemical conversion. This method used pyrolysis, hydrothermal carbonization, gasification, and torrefaction. Using this method, the process must be appropriate, depending on the type of biomass used, and the process conditions (such as heating rate, temperature, residence time). Table 1 shows the condition for making biochar.

Table 1
Process condition usig thermochemical conversion. Table was adopted from Yaashikaa *et al*., [37]

Technique	Temperature (˚C)	Residence time	Yield of biochar (%)	Yield of bio oil (%)	Syngas Production (%)
Pyrolysis	300-700 (slow)	< 2 s	35	30 (slow)	35 (slow)
	500-1000 (fast)	Hour-day(fast)	12 (fast)	75 (fast)	13 (fast)
Hydrothermal Carbonization	180-300	1-16 h	50-80	5-20	2-5
Gasification	750-900	10-20s	10	5	85
Torrefaction	290	10-60 min	80	0	20
Flash carbonization	300-600	< 30 min	37	--	--

The process condition must be ideal for getting a maximum yield of biochar. In short, when making biochar from the weight loss of the biomass, it depends on the heating condition. Water loss happens around 100°C, initially causing weight loss. Then, when reaching more than 220°C, it is followed by cellulose, hemicellulose, and lignin degradation. Simple information for the conversion of biomass using heat treatment (forming biochar) is shown in Figure 1.

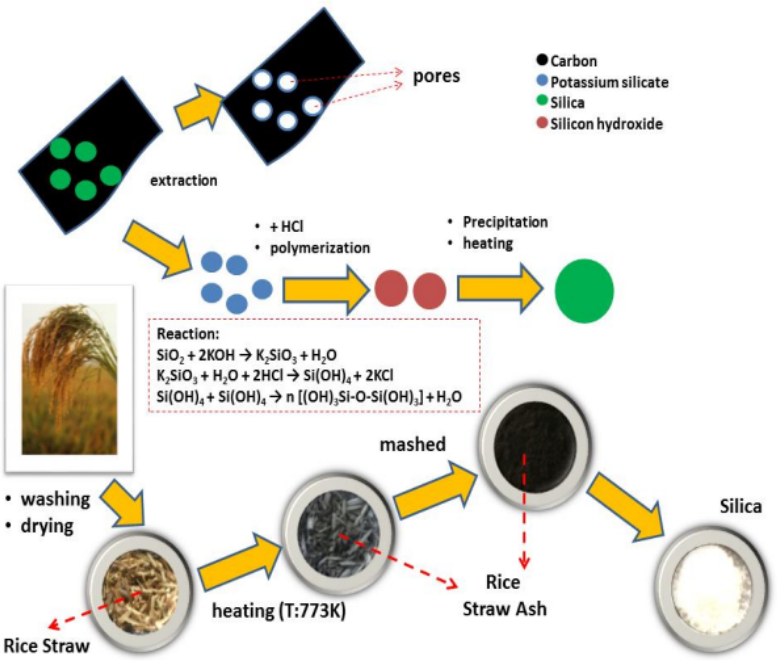

Fig. 1. The decomposition of biomass. The figure was adopted from literature by Nandiyanto and Asep Bayu Dani [26]

3. Adsorption isotherm Model

Ten adsorption isotherm models were examined to analyze the adsorption mechanism, and the calculation for gaining the curves from data fitting results are presented in Table 2. Detailed calculation on adsorption isotherm is explained in previous literature [38].

(1) Langmuir. The model assumes monolayer adsorption, where adsorbates are adsorbed to a finite number of identical and equivalent definite localized sites with no lateral interaction, supported using Equation (1):

$$\frac{1}{Qe} = \frac{1}{Qmax^{Kl}}\frac{1}{C_e} + \frac{1}{Qmax} \quad (1)$$

where K_L is the Langmuir constant, q_e is the number of molecules adsorbed at equilibrium (mg/g), and q_m is the adsorption capacity (mg/g). The adsorption factor (R_L) is expressed by Equation (2).

$$R_L = \frac{1}{1+ K_L C_e} \quad (2)$$

where RL describes: unfavorable adsorption (R_L > 1); linear adsorption (affected by the amount and concentration of adsorbed molecules) (R_L = 1); too strong adsorption or irreversible adsorption (R_L = 0); and favorable adsorption or no desorption (0 < R_L < 1).

(2) Freundlich. The model describes multilayer adsorption on heterogeneous surfaces caused by differences in adsorption heat, represented by Equation (3).

$$log\ Q_e = logk_f + \frac{1}{n} log\ \ C_e \tag{3}$$

where k_f is the Freundlich constant that estimates the adsorption capacity and C_e is the adsorbate concentration at equilibrium (mg/L). n is the degree of nonlinearity and the adsorption strength, following chemisorption (n < 1) or physisorption (n > 1); linear adsorption (a concentration-independent partition between two phases) (n = 1); normal adsorption (1/n < 1); cooperative adsorption (1/n > 1); favorable adsorption or no desorption (1 < 1/n < 0); and adsorption on a heterogeneous surface (0 < 1/n < 1; the closer to zero indicates increasing heterogeneous adsorbent surface).

(3) Temkin. This model concerns interactions between adsorbent and adsorbate, assuming that the heat of adsorption of molecules decreases linearly in each adsorbed layer and excludes high and low concentration values, represented by Equation (4).

$$q_e = B_T lnA_T + B_T lnC_e \tag{4}$$

where A_T is the equilibrium constant of the Temkin model. $б_T$ is the Temkin constant, informing physical ($б_T$ < 8 kJ) or chemical ($б_T$ > 8 kJ) adsorption.

(4) Dubinin-Radushkevich. This model is based on the adsorption of gases by porous adsorbents and the pore-filling mechanism, represented by Equation (5).

$$lnq_e = lnq_s - (\beta\varepsilon^2) \tag{5}$$

where q_s is the saturation capacity (mg/g) and $б$ is the Dubinin-Radushkevich constant correlating to the average free adsorption energy. ε is the Polanyi potential associated with equilibrium conditions, in which the value correlates to adsorption energy (E) (see Equation (6) and (7):

$$\varepsilon = RTln\left[1 + \frac{1}{C_e}\right] \tag{6}$$

$$E = \frac{1}{\sqrt{2\beta}} \tag{7}$$

E relates to the physical (E < 8 kJ) or chemical (E > 8 kJ) adsorption

(5) Flory-Huggins. This model represents multilayer adsorption on the pore surface of the adsorbent, described in Equation (8).

$$log\ \frac{\theta}{Ce} = log\ K_{FH} + n\ log\ (1 - \theta) \tag{8}$$

where $\theta = \left(1 - \frac{C_e}{C_o}\right)$ is the degree of monolayer coverage. n_{FH} and K_{FH} are the equilibrium constant for the Flory-Huggins model, in which it correlates to the Gibbs free energy ($\Delta G°$), as presented in Equation (9):

$$\Delta G° = -RT\ ln\ K_{FH} \quad (9)$$

The $\Delta G°$ can describe the spontaneous and temperature-dependent nature of the adsorption when it is negative.

(6) Fowler- Guggenheim. This model considers the lateral interaction of adsorbed molecules during the adsorption, explicitly explained by Equation (10).

$$K_{FG}C_e = \frac{\theta}{1-\theta} exp\ (\frac{2.\theta.W}{RT}) \quad (10)$$

where K_{FG} is the Fowler-Guggenheim constant (L/mg). W is the interaction energy between the adsorbed molecules (kJ/mol), informing processes under exothermic (W > 0), endothermic (W < 0 kJ/mol), or no interaction between adsorbed molecules (W = 0 kJ/mol).

(7) Hill Deboer. This model represents mobile adsorption and lateral interactions between the molecules that have been adsorbed based on the values of the model's parameters, in expressed Equation (11).

$$K_1.C_e = \frac{\theta}{1-\theta} exp\ (\frac{\theta}{1-\theta} - \frac{K_2\theta}{RT}) \quad (11)$$

where K_1 (L/mg) and K_2 (kJ/mol) are the contact energy constants for the adsorbed molecules, informing exothermic with intermolecular adsorption (K_2 > 0); endothermic with repulsion (K_2 < 0), or no interaction between adsorbates (K_2 = 0).

(8) Jovanovic. The model is based on the phenomena observed in the Langmuir model, but it does not allow mechanical contact between the adsorbate and adsorbent (presented in Equation (12):

$$lnQ_e = lnQ_{max} - K_jC_e \quad (12)$$

where Q_e is the amount of adsorbate in the adsorbent at equilibrium (mg/g), Q_{max} is the maximum absorption of the adsorbate, and K_J is the Jovanovic constant.

(9) Harkin Jura. The model evaluates adsorption on a heterogeneous surface where a multilayer form during the adsorption, represented in Equation (13):

$$\frac{1}{q_e^2} = \frac{B_{HJ}}{A_{HJ}} - \left(\frac{1}{A}\right) logC_e \quad (13)$$

where B_{HJ} is related to the specific surface area of the adsorbent and A_{HJ} is the Harkin-Jura constant.

(10) Halsey. This model evaluates the multilayer adsorption system at a relatively large distance from the surface. Similarly, to the Freundlich model, the Halsey model applies to both multilayer adsorption and heterogeneous surfaces with non-uniformly distributed adsorption heat, represented in Equation (14):

$$Q_e = \frac{1}{n_H} lnK_H - \left(\frac{1}{n_H}\right) lnC_e \quad (14)$$

where K_H and n are the Halsey's constants.

Table 2
Parameters, calculations, and data fitting for adsorption isotherms

Isotherm Model	Linear Equation	Plotting		Parameters
		x-Axis	y-Axis	
Langmuir	$\frac{1}{Qe} = \frac{1}{QmaxK_L}\frac{1}{Ce} + \frac{1}{Qmax}$	$\frac{1}{C_e}$	$\frac{1}{Q_e}$	• $\frac{1}{Q_{max}} = intercept$ • $K_L = \frac{1}{Q_{max} \times slope}$
Freundlich	$Q_e = ln\, k_f + \frac{1}{n}C_e$	lnC_e	lnQ_e	• $lnK_F = intercept$ • $\frac{1}{n} = slope$
Temkin	$q_e = B_T A_T + B_T Ce$	lnC_e	Q_e	• $B = slope$ • $B_T lnA_T = intercept$ • $B_T = \frac{RT}{B}$
Dubinin-Radushkevich	$q_e = q_s - (\beta\varepsilon^2)$	ε^2	lnQ_e	• $\beta = K_{DR} = slope$ • $E = \frac{1}{\sqrt{2 \times K_{DR}}}$
Flory Huggins	$log\frac{\theta}{C_e} = logK_{FH} + nlog\,(1-\theta)$	$log\ log\left(\frac{\theta}{C_0}\right)$	$log(1-\theta)$	• $n_{FH} = slope$ • $k_{FH} = intercept$ • $\Delta G^{o} = RTln(k_{FH})$ $\theta = 1 - (\frac{C_e}{C_0})$
Fowler-Guggenheim	$ln\left(\frac{C_e(1-\theta)}{\theta}\right) - \frac{\theta}{1-\theta} = -lnK_{FG} + \frac{2W\theta}{RT}$	θ	$ln\left[\frac{C_e(1-\theta)}{\theta}\right]$	• $W = slope$ • $-lnK_{FG} = intercept$ • $\alpha\ (slope) = \frac{2W\theta}{RT}$ $\theta = 1 - (\frac{C_e}{C_0})$
Hill-Deboer	$ln\left[\frac{C_e(1-\theta)}{\theta}\right] - \frac{\theta}{1-\theta} = -lnK_1 - \frac{K_2\theta}{RT}$	θ	$ln\left[\frac{C_e(1-\theta)}{\theta}\right] - \frac{\theta}{1-\theta}$	• $-lnk_1 = intercept$ • $\alpha\ (slope) = \frac{k_2\theta}{RT}$ • $\theta = 1 - (\frac{C_e}{C_0})$
Jovanovic	$lnq_e = lnq_{max} - K_J C_e$	C_e	lnQ_e	• $K_J = slope$ • $lnq_{max} = intercept$
Harkin-Jura	$\frac{1}{q_e^2} = \frac{B}{A} - \left(\frac{1}{A}\right) logC_e$	$logC_e$	$\frac{1}{q_e^2}$	• $A_H = \frac{1}{Slope}$ • $\frac{B_H}{A_H} = intercept$
Halsey	$lnQ_e = \frac{1}{n_H} lnK_H - \frac{1}{n} lnC_e$	lnC_e	lnQ_e	• $\frac{1}{n} = slope$ • $\frac{1}{n} lnK_H = intercept$

3. Methodology

3.1 Fabrication of Carbon-based Adsorbents

Carbon microparticles were prepared by carbonizing 250 g of tamarind seed waste using an electric furnace at 250°C for 5 hours. Before the carbonization, the seed was washed (using ultrapure water to remove dust and impurities), dried naturally using sunlight for 2 days, saw milled using the apparatus used in our previous study [20], and sieving test (Yayasan Bumi Publikasi Nusantara, Indonesia, hole variations of 2000, 1000, 500, 250, 125, 99, 74 µm; to classify and determine the size of particles).

3.2 Characterization of Carbon-based Adsorbents

The surface morphology of the particles was examined using a Digital Microscope (BXAW-AX-BC, China). Analysis of the functional group of the prepared carbon was performed using Fourier Transform Infrared (FTIR-4600, Jasco Corp., Japan).

3.3 Adsorption Experimental

In the adsorption experiment (a glass batch reactor with a total volume of 1 L), curcumin in aqueous solutions (concentrations of 20, 40, 60, 80, and 100 ppm) was mixed with 0.5 g of the prepared carbon particles (specific sizes of 2000, 1000, and 500 µm) for 24 hours (in the dark condition). Blank solutions (curcumin solution without additional carbon) at various concentrations were also tested using the same process condition and used as a standard comparison. During the adsorption, an aliquot sample (3 mL) was taken at specific hours and tested using a visible spectrophotometer (Model 7205 JENWAY; Cole-Parmer; US), and the measurement curve results were normalized and put in the Lambert-Beer formula to obtain actual concentration at the specific hour. Detailed information for the measurement analysis using visible measurement is reported elsewhere [39, 40].

4. Results

4.1 Characterization of Carbon-based Adsorbents

The surface morphology of carbon particles from tamarind seeds is presented in Figure 2 (a), and the Ferret size analysis is shown in Figure 2(b). Carbon particles with irregular shapes have sizes of between 500 and 1000 µm with an average size of 1129.93 µm. To get the precise size, the particles were then put into a sieving process, in which the particles with sizes of 500, 1000, and 2000 µm can be obtained and used for further analysis. Figure 2(c) is the result of the FTIR characterization of the prepared carbon microparticles from tamarind seeds. Carbon particles of different sizes have identical peaks, and the main focused peaks are determined in the red dashed area in Figure 2(c), confirming that the saw-milling process did not alter the chemical structure of the material. Several peaks were obtained, informing the carbon material, including the -OH group at a wavelength of 3650-3250 cm^{-1}, the C=O group in the stretching vibration at a wavelength of 1612-1651 cm^{-1}, the C-O group in the stretching vibration at a wavelength of 1041-1200 cm^{-1}, and the C-H group with bending vibrations at wavelength 1315-1455 cm^{-1}. The crystallinity of the material was not focused on in this study, and all subsequent processes involving adsorption are assumed to be dependent only on the size of the carbon adsorbent [41-44].

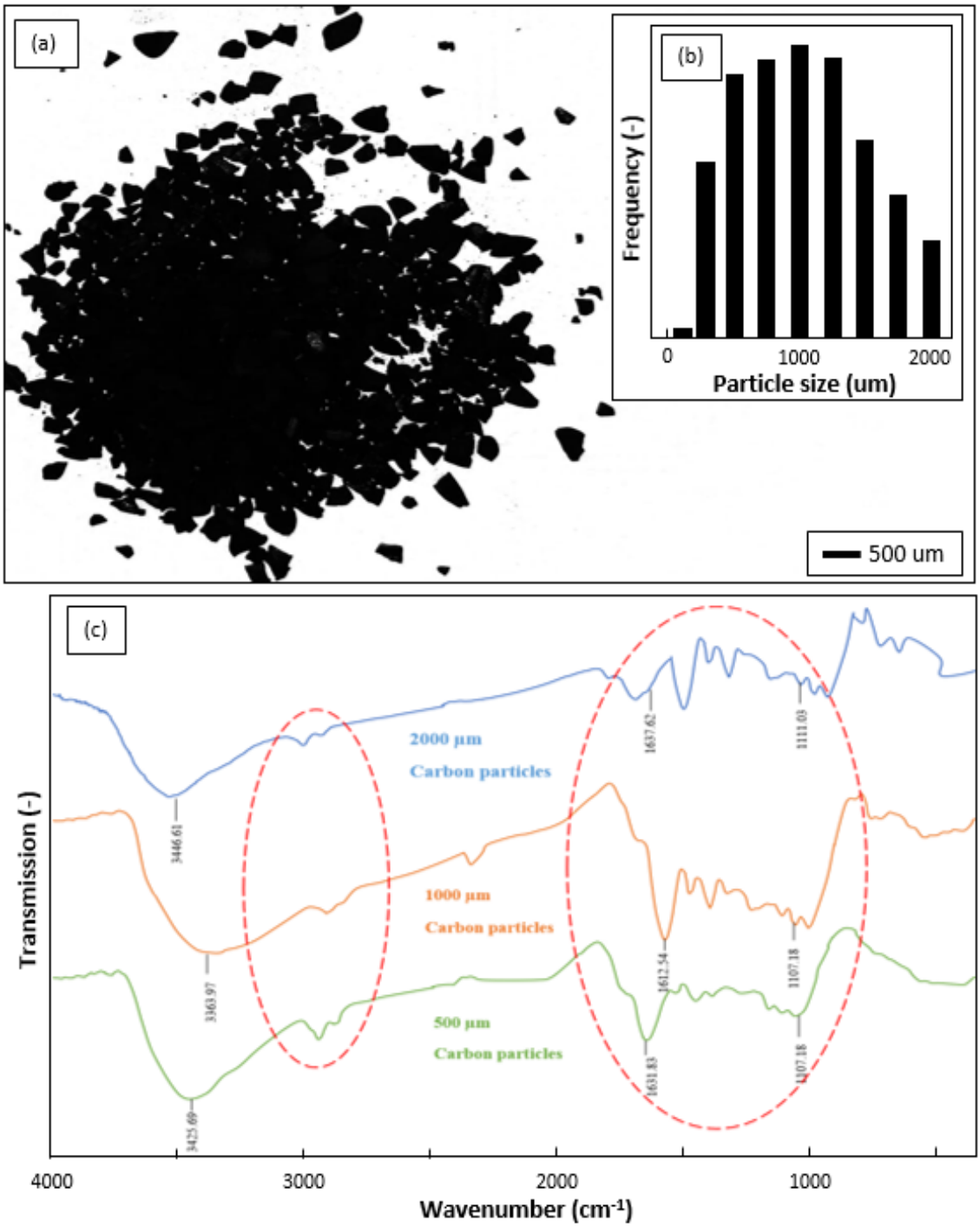

Fig. 2. Microscope images of carbon particles (a) with their size distribution (b). Figure (c) is the FTIR analysis results of carbon with different sizes

4.2 Adsorption of Carbon-based Adsorbents

Figure 3(a) shows the Visible spectra of curcumin solution during adsorption. Due to the deterioration of curcumin concentration during adsorption, the absorbance at all wavelengths decreased over time. The visualization of the decreasing concentration of curcumin is shown in Figure 3(b), where the yellow color of the solution becomes transparent gradually. Analysis based on Beer's Law the absorbance can be re-expressed as a unit of concentration (see Figure 3(c) and (d)).

Degradation was measured for 24 hours of the adsorption, which was an ample amount of time to observe the differences in the adsorption performances under various carbon adsorbent parameters. As a comparison, we also evaluated the sample without any additional carbon adsorbent (see black-dashed lines in each figure). To confirm the influence of parameters on the adsorption performance empirically, the Langmuir–Hinshelwood kinetic model for solid–solute interaction was employed, expressed by involving C_e and several constants (i.e. the apparent rate constant (k_T), and the apparent equilibrium constant for adsorption of the molecule on the adsorbent surface (Kc)), as presented in Equation (15) [45]:

$$-\frac{dC_e}{dt} = \frac{k_T.K_C.C_e}{1+ K_C.C_e} \quad (15)$$

Since K_C relates to the number of adsorbate species such as water (H_2O), hydroxide ($OH-$), and oxygen (O_2) as well as the process uses a very low amount of curcumin (100 ppm) and the amount of adsorbate is assumed to constant during the adsorption, Equation (15) can be rewritten to a first-order reaction correlation by assuming $1 + K_C \cdot C \approx 1$. From this correlation, the kinetics of adsorption can be described, and all calculation results are paneled in each curve in Figure 3(c) and (d).

Curcumin decreasing rates relied on the size of the carbon adsorbent utilized (see Figure 2(c)). The amount of curcumin without additional adsorbent displayed insignificant discoloration with the final concentration of 98%, which can be ignored. A slight change in the concentration was found when using adsorbents with different sizes. The use of carbon adsorbent with sizes of 2000, 1000, and 500 μm gave results in the final amount of curcumin of about 87, 75, and 60, respectively, promoting the adsorption rates of 0.83×10^{-3}; 0.91×10^{-3}; and 1.11×10^{-3} min^{-1}. In short, the fastest discoloration of curcumin was achieved when utilizing adsorbent with smaller sizes, confirming the important roles of the size on the surface-active area for adsorption.

The normalized curcumin amounts concerning the effect of initial curcumin loadings on the adsorption performance over time are presented in Figure 3(d). Constant adsorbent particle size (i.e. 500 μm) was used to verify that the adsorption rate is from the effect of the size. Different curcumin loadings seemed to have an impact on the adsorption. Curcumin loadings of 100, 80, 60, 40, and 20 ppm resulted in the process with the final concentration/adsorption efficacy of 61 ppm/61%; 54 ppm/68%; 42 ppm/69%; 27 ppm/69%; and 15 ppm/77%, respectively. The adsorption rates for curcumin loading of 100, 80, 60, 40, and 20 ppm were 1.11×10^{-3}; 0.96×10^{-3}; 0.97×10^{-3}; 0.98×10^{-3}; and 0.86×10^{-3} min^{-1}, respectively. The results showed that the additional adsorbent correlated to the adsorption rate, which can be discussed:

(i) Increasing curcumin loading has a positive correlation with the adsorption rate. The more curcumin amount involved results in more contact with the adsorbent. Adsorbate-adsorbent interaction makes more possibilities for adsorption.
(ii) Too high amount of curcumin added has limitations in the existence of a high concentration of un-adsorbed curcumin solution. Indeed, to increase total adsorption efficacy, additional multi-step adsorption should be done.
(iii) Too less amount of curcumin has an impact on the limitations of the adsorbent-adsorbate interaction. Thus, less amount of curcumin can be adsorbed. To increase the efficacy in the adsorption, an additional mixing process can be implemented, but it should be considered regarding the desorption of curcumin and the breakup of the adsorbent physical structure.

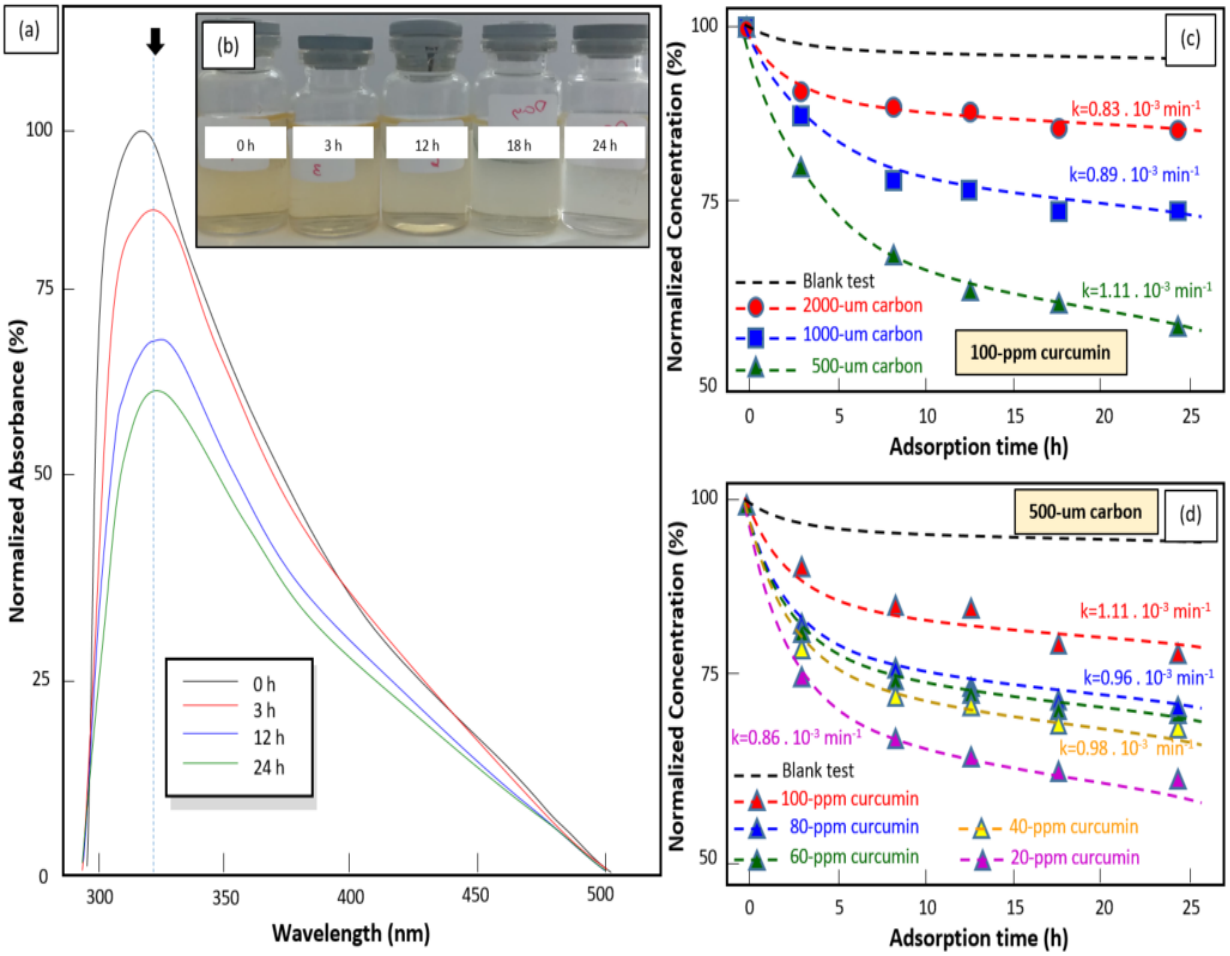

Fig. 3. (a) Visible spectrophotometer results; (b) photograph images of samples during the adsorption; (c) Kinetic analysis as a function of adsorbent size; and (c) Kinetic analysis as a function of curcumin loading

The relationship between the initial adsorbate loading and the adsorption capacity of carbon is illustrated in Figure 4. As confirmed in the above results in Figure 3(d), the adsorption capacity increases when the initial adsorbate loading increases. At a high initial concentration, the adsorbent active site will be surrounded by more adsorbate molecules. Thus, the adsorption capacity increases with the increasing initial loading of adsorbate molecules. At a low initial adsorbate concentration, the amount of adsorbate adsorbed to the accessible adsorbent active sites is low. These results indicate that the initial adsorbate concentration is an important factor affecting the adsorption capacity of carbon. Indeed, with an increase in the initial adsorbate loading, the adsorption sites on the carbon surface are quickly surrounded by more adsorbate molecules, increasing the mass transfer of the adsorbate to the surface of the adsorbent, thereby increasing the adsorption capacity [45-47].

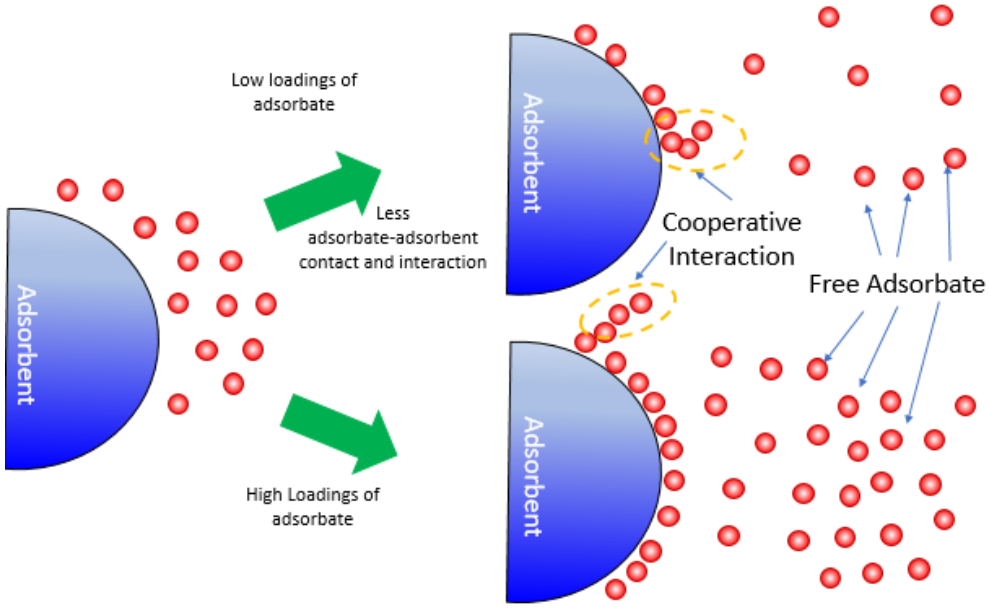

Fig. 4. Effect of initial adsorbate concentration on the adsorption capacity

To understand further analysis of the phenomena happening during the adsorption, adsorption isotherm is evaluated and achieved by comparing the adsorption results and the adsorption isotherm models (see Table 3). Based on the analysis of the R2 fitting results, the adsorption of curcumin by various particle sizes of carbon showed compatibility with the Halsey > Jovanovic > Harkin Jura > Temkin > Langmuir models. Detailed proposed adsorption mechanism based on the adsorption isotherm model is illustrated in Figure 5(a) and (b).

The adsorption mechanism when using a small adsorbent (i.e. size of 500 µm) is depicted in Figure 4(a), revealing the existence of the monolayer adsorption on the adsorbent surface (confirmed by Halsey, Jovanovic, Harkin Jura, Temkin, and Langmuir models) with pore-filling characteristics (confirmed by the Dubinin-Radushkevich model), cooperative interaction (confirmed by Freundlich model), and physisorption characteristics (confirmed by Freundlich, Temkin, Dubinin-Radushkevich model). The interaction between the adsorbent surface and the adsorbate occurs physically, involving weak interactions originating from Van der Waals forces.

Meanwhile, a different phenomenon happened for the adsorption mechanism when using large adsorbents (i.e. 1000 and 2000 µm), illustrated in Figure 5(b). During the adsorption, a monolayer surface was formed (confirmed by the Halsey, Jovanovic, Harkin Jura, Temkin, Hill Deboer, and Langmuir models). Furthermore, further phenomena were found for the existence of the combination of physisorption and chemisorption interactions (cooperative interactions) between the adsorbates. At the same time, the adsorption also occurred on the multilayer surface (confirmed by Flory Huggins). The adsorption mechanism also follows the pore-filling characteristics (confirmed by Dubinin Radushkevich's model) and physisorption characteristics (confirmed by Freundlich, Temkin, and Dubinin Radushkevich models) (see Figure 5(b)). An additional consideration is the presence of non-spontaneous adsorption due to the positive value of the Gibbs free energy. Thus, to enhance adsorption, additional external forces such as temperature and pressure are required. This hypothesis is also strengthened by the Flower Huggins Guggenheim isotherm parameter which shows a value of $W < 0$.

Table 3
Detailed data of adsorption isotherm parameters

Model	Parameter	Particle size (µm)			Note
		2000	1000	500	
Freundlich	R^2	0.5791	0.6895	0.6974	Monolayer formation (R^2 < 0.70) on the adsorbent surface.
	K_f	2.923	2.946	5.675	Freundlich constant of adsorption isotherm
	n	1.428	1.121	1.01	Physisorption process (n > 1)
	1/ n	1.072	1.081	1.739	Favorable cooperative adsorption
Langmuir	R^2	0.9701	0.8118	0.9362	The presence of monolayer adsorbent surface
	Q_{max}	76.335	588.235	78.125	Maximum capacity of adsorbent (mg/g)
	R_L	0.391	0.786	0.393	Favorable adsorption (0 < 1/n < 1)
	K_L	0.017	2.070 10^{-3}	1.000	Constants Langmuir model
Temkin	R^2	0.9974	0.9790	0.9506	Monolayer (R^2 > 0.70) on the adsorbent surface.
	A_T (L/g)	76.335	588.235	588.235	Binding constant for the Temkin equilibrium
	$б_T$ (J/mol)	59.274	54.967	32.353	Physical process adsorption ($б_T$ > 8 kJ/mol)
Dubinin-Radushkevich	R^2	0.9494	0.7608	0.8659	The adsorbent surface has micropores (R^2 > 0.70).
	Qs (mg/g)	1.545	1.254	1.350	Adsorbent's capacity for adsorption
	$б$ (mol^2/kJ^2)	0.0022	0.0025	0.003	The Dubinin-Radushkevich constant
	E (kJ/mol)	0.321	0.282	0.278	Physical interaction between adsorbate molecules
Flory Huggins	R^2	0.920823382	0.772970058	0.657014847	● Multilayer adsorption (R^2 > 0.7) ● Monolayer adsorption (R^2 < 0.7)

	n_{FH}	1.345	0.6222	-0.2408	● Adsorbate is present in more than one active adsorbent zone (n_{FH} < 1) ● multilayer of adsorbate molecules formation (n_{FH} > 1)
	K_{FH} (L/mg)	22.130	1.944	0.385	Flory Huggins constant
	$\Delta G°$ (kJ/mol)	7.029	1.498	-2.166	● Spontaneous adsorption ($\Delta G°$ < 0) ● Non-spontaneous adsorption ($\Delta G°$ > 0)
Fowler-Guggenheim	R^2	0.997183007	0.883144203	0.487206207	● Monolayer adsorption (R^2 < 0.7) ● Multilayer adsorption (R^2 > 0.7)
	K_{FG} *(L/mg)*	4.486	0.270	0.027	Constants for the Fowler-Guggenheim model
	W (kJ/mol)	-28.642	-10.271	-55.676	W < 0 kJ/mol, the interaction between adsorbed molecules will be repulsive
Hill Deboer	R^2	0.98706509	0.854600071	0.93275497	Monolayer adsorption (R^2 > 0.7)
	K_1 (L/mg)	0.040	0.201	0.026	Constant for the Hill-Deboer model
	K_2 (L/ mg)	278.642	637.000	294.875	Attraction between adsorbed species
Jovanovic	R^2	0.997416244	0.979085848	0.950685754	Monolayer adsorption (R^2 > 0.7)
	K_J (L/mg)	0.9678	0.881	0.5035	Constants for the Jovanovic model
	Qmax (mg/g)	6.675	7.174	3.706	Maximum capacity of adsorbent (mg/g)
Harkin Jura	R^2	0.990433932	0.968627831	0.870784776	Monolayer adsorption (R^2 > 0.7)
	A_{HJ}	0.035	0.027	0.086	Constants for the Harkin-Jura model
	B_{HJ}	0.234	0.329	0.489	Relates to the surface area of the adsorbent
Halsey	R^2	0.998	0.998	0.998	Monolayer adsorption (R^2 > 0.7)

	n	1.0	1.0	1.0	Constants for the Halsey model
	K_H	0.399	0.399	0.399	Constants for the Halsey model

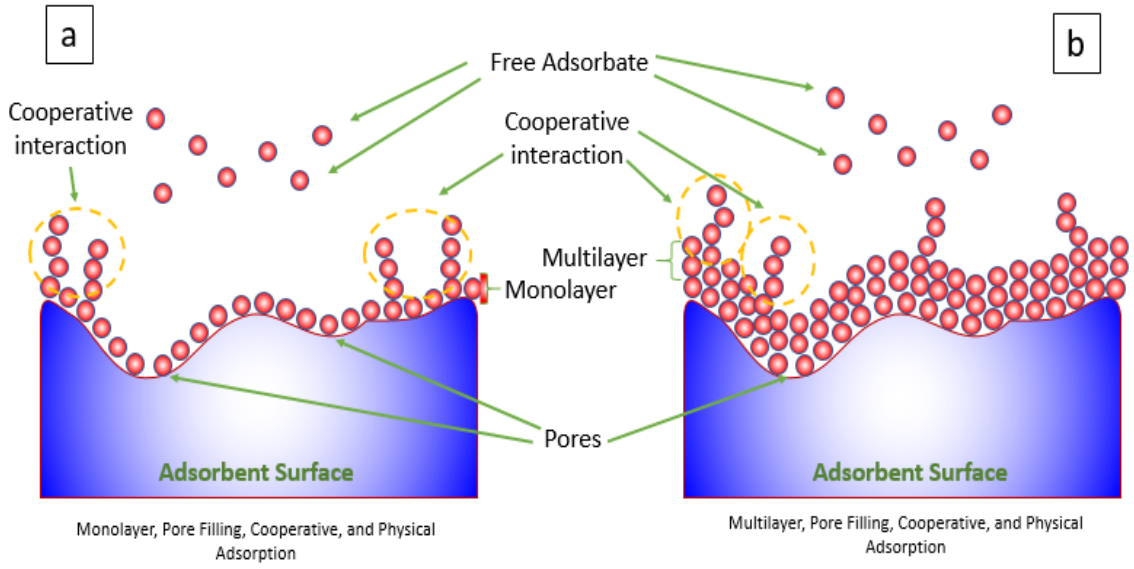

Fig. 5. Adsorption mechanism for small (a) and large (b) adsorbent

5. Conclusions

Carbon materials derived from tamarind seeds are developed and used as adsorbents for the adsorption of dyes from aqueous solutions at low sorbate concentrations, which can support the need for a sustainable environment and clean water for assisting sustainable development goals (SDGs) in developing countries The adsorption equilibrium data were matched, which was confirmed to 10 isotherm models, namely Langmuir, Freundlich, Temkin, Dubinin-Radushkevich, Flory Huggins, Fowler–Guggenheim, Hill Deboer, Jovanovic, Harkin Jura, and Halsey by analyzing the value of the correlation coefficient. Adsorption occurs via the formation of a monolayer with a physisorption characteristic binding energy caused by the presence of a Van der Waals force, in which the main causes of the formation of monolayers are geometric irregularities and energy inhomogeneity of the surface profile. Based on the results, carbon-based products' good adsorption mechanism and low cost indicate that they can be used as effective adsorbents for water purification while also protecting the environment.

Acknowledgment

This study was supported by RISTEK BRIN and Universitas Pendidikan Indonesia (Grant: Bangdos).

References

[1] Nandiyanto, Asep Bayu Dani, Ajeng Sukmafitri, Risti Ragadhita, Rosi Oktiani, Nuria Haristiani, and Ida Hamidah. "Conventional filter for the water treatment system in rural area". *Journal of Engineering Science and Technology* 14, no. 4 (2019): 2090-2097.

[2] Maryanti, Rina, Nur Indri Rahayu, Muktiarni, Dwi Fitria Al Husaeni, Achamd Hufad, Sunardi, and Asep Bayu Dani Nandiyanto. "Sustainable development goals (SDGs) in science education: Definition, literature review, and bibliometric analysis." *Journal of Engineering Science and Technology* 17 (2022): 161-181.

[3] Nandiyanto, Asep Bayu Dani, Meli Fiandini, Siti Nur Hofifah, Risti Ragadhita, Dwi Fitria Al Husaeni, Dwi Novia Al Husaeni, Rina Maryanti, and Alias Masek. "Collaborative practicum with experimental demonstration for teaching the concept of production of bioplastic to vocational students to support the sustainability development goals." *Journal of Technical Education and Training* 14, no. 2 (2022): 1-13. https://doi.org/10.30880/jtet. 2022.14.02.001

[4] Jayasree, R., P Senthil Kumar, A Saravanan, R V Hemavathy, P R Yaashikaa, P Arthi, J Shreshta, S Jeevanantham, Karisham S, Mariadhas Valan Arasu, Naif Abdullah Al-Dhabi, and Ki Choon Choi. "Sequestration of toxic Pb (II) ions using ultrasonic modified agro waste: Adsorption mechanism and modelling study." *Chemosphere* 285 (2021): 131502. https://doi.org/10.1016/j.chemosphere.2021.131502

[5] Camargo-Perea, Ana L., Ainhoa Rubio-Clemente, and Gustavo A. Peñuela. "Use of ultrasound as an advanced oxidation process for the degradation of emerging pollutants in water." *Water* 12, no. 4 (2020): 1068. https://doi.org/10.3390/w12041068

[6] Cui, Hongmei, Xing Huang, Zhongchen Yu, Ping Chen, and Xiaoling Cao. "Application progress of enhanced coagulation in water treatment." *RSC advances* 10, no. 34 (2020): 20231-20244. https://doi.org/10.1039/D0RA02979C

[7] Nandiyanto, Asep Bayu Dani. "Isotherm adsorption of carbon microparticles prepared from pumpkin (Cucurbita maxima) seeds using two-parameter monolayer adsorption models and equations." *Moroccan Journal of Chemistry* 8, no. 3 (2020): 8-3. https://doi.org/10.48317/IMIST.PRSM/morjchem-v8i3.21636

[8] Nandiyanto, Asep Bayu Dani, Risti Ragadhita, and Jumril Yunas. "Adsorption isotherm of densed monoclinic tungsten trioxide nanoparticles." *Sains Malaysiana* 49, no. 12 (2020): 2881-2890. http://dx.doi.org/10.17576/jsm-2020-4912-01

[9] Otieno, Benton, Seth Apollo, John Kabuba, Bobby Naidoo, and Aoyi Ochieng. "Ozonolysis post-treatment of anaerobically digested distillery wastewater effluent." *Ozone: Science & Engineering* 41, no. 6 (2019): 551-561. https://doi.org/10.1080/01919512.2019.1593818

[10] Peng, Hao, and Jing Guo. "Removal of chromium from wastewater by membrane filtration, chemical precipitation, ion exchange, adsorption electrocoagulation, electrochemical reduction, electrodialysis, electrodeionization, photocatalysis and nanotechnology: a review." *Environmental Chemistry Letters* 18 (2020): 2055-2068. https://doi.org/10.1007/s10311-020-01058-x

[11] Ragadhita, Risti, and Asep Bayu Dani Nandiyanto. "Curcumin adsorption on zinc imidazole framework-8 particles: Isotherm adsorption using Langmuir, Freundlich, Temkin, and Dubinin-Radushkevich models." *Journal of Engineering Science and Technology* 17, no. 2 (2022): 1078-1089.

[12] Tian, Jiayu, Xingrui Zhao, Shanshan Gao, Xiaoying Wang, and Ruijun Zhang. "Progress in research and application of nanofiltration (nf) technology for brackish water treatment." *Membranes* 11, no. 9 (2021): 662. https://doi.org/10.3390/membranes11090662

[13] Akpomie, Kovo G., Jeanet Conradie, Kayode A. Adegoke, Kabir O. Oyedotun, Joshua O. Ighalo, James F. Amaku, Chijioke Olisah, Adedapo O. Adeola, and Kingsley O. Iwuozor. "Adsorption mechanism and modeling of radionuclides and heavy metals onto ZnO nanoparticles: A review." *Applied Water Science* 13, no. 1 (2023): 20. https://doi.org/10.1007/s13201-022-01827-9

[14] Anshar, Andi Muhammad, Paulina Taba, and Indah Raya. "Kinetic and thermodynamics studies the adsorption of phenol on activated carbon from rice husk activated by ZnCl2". *Indonesian Journal of Science and Technology* 1, no. 1 (2016): 47-60. https://doi.org/10.17509/ijost.v1i1.2213

[15] Awan, Muhammad Maqbool Sadiq, Parviz Soroushian, Arshad Ali, and Muhammad Yousaf Saqid Awan. "High-performance cementitious matrix using carbon nanofibers. " *Indonesian Journal of Science and Technology* 2, no. 1 (2017): 57-75. https://doi.org/10.17509/ijost.v2i1.5989

[16] Awan, Muhammad Maqbool Sadiq, Parviz Soroushian, Arshad Ali, and Muhammad Yousaf Saqid Awan. "Use of carbon nano-fibers in cementitious mortar". *Indonesian Journal of Science and Technology* 2, no. 2 (2017): 134-151. https://doi.org/10.17509/ijost.v2i2.8001

[17] Asmara, Y.P., and Tedi Kurniawan. Corrosion prediction for corrosion rate of carbon steel in oil and gas environment: A review. *Indonesian Journal of Science and Technology* 3, no. 1 (2018): 64-74. https://doi.org/10.17509/ijost.v3i1.10808

[18] Awan, Maqbool S, Arshad Ali, Perviz S, and Yousaf S Awan. "Carbon nano fibre reinforcements in concrete." *Indonesian Journal of Science and Technology* 4, no. 1 (2019): 1-16. https://doi.org/10.17509/ijost.v4i1.4140

[19] Khuluk, Rifki Husnul, Ali Rahmat, Buhani, and Suharso. "Removal of methylene blue by adsorption onto activated carbon from coconut shell (*Cocous nucifera L.).*" *Indonesian Journal of Science and Technology* 4, no. 2 (2019): 229-240. https://doi.org/10.17509/ijost.v4i2.18179

[20] Efiyanti, Lisna, Dian Anggraini Indrawan, Zulhan Arif, Devandri Hutapea, and Ane Dwi Septina. "Synthesis and application of a sulfonated carbon catalyst for a hydrolisis reaction." *Indonesian Journal of Science and Technology* 5, no. 3 (2020): 410-420. https://doi.org/10.17509/ijost.v5i3.25275

[21] Kartikowati, Christina Wahyu, Aditya Farhan Arif, Osi Arutanti, and Takashi Ogi. "Carbon-coated single-phase Ti4O7 nanoparticles as electrocatalyst support." *Indonesian Journal of Science and Technology* 6, no. 1 (2021): 235-242. https://doi.org/10.17509/ijost.v6i1.32519

[22] Sambudi, N.S., Sithambaran, Y., Hui, K.C., Nugraha, M.W., Kamal, N.A., Harun, N.Y., and Sufian, S. "Modification of kaolin with carbon quantum dots as composite for methylene blue removal: Literature review and experiment." *Indonesian Journal of Science and Technology* 7, no. 2 (2022): 311-336. https://doi.org/10.17509/ijost.v7i2.50810

[23] Nandiyanto, Asep Bayu Dani, Meli Fiandini, Risti Ragadhita, and Muhammad Aziz. "How to purify and experiment with dye adsorption using carbon: Step-by-step procedure from carbon conversion from agricultural biomass to concentration measurement using UV Vis spectroscopy." *Indonesian Journal of Science and Technology* 8, no. 3 (2023): 363-380. https://doi.org/10.17509/ijost.v8i3.58290

[24]. N'diaye, Abdoulaye Demba. "Nonlinear analysis of the kinetics and equilibrium for adsorptive removal of paranitrophenol by powdered activated carbon." *ASEAN Journal of Science and Engineering* 3, no. 3 (2023): 271-280. https://doi.org/10.17509/ajse.v3i3.49136

[25] Ragadhita, Risti, and Nandiyanto Asep Bayu Dani. "Why 200°C is effective for creating carbon from organic waste (from thermal gravity (TG-DTA) perspective)?." *ASEAN Journal for Science and Engineering in Materials* 2, no. 2 (2023): 75-80.

[26] Nandiyanto, Asep Bayu Dani. "Cost analysis and economic evaluation for the fabrication of activated carbon and silica particles from rice straw waste." *Journal of Engineering, Science and Technology* 13, no. 6 (2018): 1523-1539.

[27] Sukmafitri, Ajeng, Risti Ragadhita, Nandiyanto Asep Bayu Dani, Nugraha, Wily Cahya, and Mulyanti, Budi. Effect of pH condition on the production of well-dispersed carbon nanoparticles from rice husks. *Journal of Engineering, Science and Technology*, 15 no. 2 (2020): 991-1000.

[28] Emmanuel, Jwanan Luther, Mustapha Omenesa Idris, Idris, Abdulmutalib Omeiza Usman, Quasim Musa, Suleiman, Panfo Sambo. "Biomass-Derived Activated Carbon: A Viable Material for Remediation of pb2+ and 2, 4-Dichlorophenol (2, 4 DCP) through Adsorption." *Journal of Advanced Research in Applied Sciences and Engineering Technology* 25, no. 1 (2021): 37-45. https://doi.org/10.37934/araset.25.1.3745

[29] Nandiyanto, Asep Bayu Dani, Meli Fiandini, Denaya Ayu Fadiah, Pitri Aprilia Muktakin, Risti Ragadhita, Willy Cahya Nugraha, Teguh Kurniawan, Muhammad Roil Bilad, Jumril Yunas, Abdulkareem Sh. Mahdi Al Obaidi. "Sustainable biochar carbon microparticles based on mangosteen peel as biosorbent for dye removal: Theoretical review, modelling, and adsorption isotherm characteristics." *Journal of Advanced Research in Fluid Mechanics and Thermal Sciences* 105, no. 1 (2023): 41-58. https://doi.org/10.37934/arfmts.105.1.4158

[30] Nurrahma, Arinal Haq Izzawati, Hana Haruna Putri, and Ray March Syahadat. "Scientific research trends of flooding stress in plant science and agriculture subject areas (1962-2021)." *ASEAN Journal of Science and Engineering* 3, no. 2 (2023): 163-178

[31] Nandiyanto, Asep Bayu Dani, Gabriela Chelvina Santiuly Girsang, Rina Maryanti, Risti Ragadhita, Sri Anggraeni, Fajar Miraz Fauzi, Putri Sakinah et al. "Isotherm adsorption characteristics of carbon microparticles prepared from pineapple peel waste." *Communications in Science and Technology* 5, no. 1 (2020): 31-39. https://doi.org/10.21924/cst.5.1.2020.176

[32] Fiandini, Meli, Risti Ragadhita, Asep Bayu Dani Nandiyanto, and Willy Cahya Nugraha. "Adsorption characteristics of submicron porous carbon particles prepared from rice husk." *Journal of Engineering Science and Technolog* 15 (2020): 022-031.

[33] Nandiyanto, Asep Bayu Dani, Zulfan Adi Putra, Riezqa Andika, Muhammad Roil Bilad, Tedi Kurniawan, Rizka Zulhijah, and Ida Hamidah. "Porous activated carbon particles from rice straw waste and their adsorption properties." *Journal of Engineering Science and Technology* 12, no. 8 (2017): 1-11.

[34] Nandiyanto, Asep Bayu Dani, Zulfa Fathi Arinalhaq, Salma Rahmadianti, Mauseni Wantika Dewi, Yulian Putri Chandra Rizky, Aulia Maulidina, Sri Anggraeni, Muhammad Roil Bilad, and Jumril Yunas. "Curcumin Adsorption on Carbon Microparticles: Synthesis from Soursop (*AnnonaMuricata* L.) Peel Waste, Adsorption Isotherms and Thermodynamic and Adsorption Mechanism." *International Journal of Nanoelectronics & Materials* 13 (2020).

[35] Nandiyanto, Asep Bayu Dani, Rina Maryanti, Meli Fiandini, Risti Ragadhita, Dian Usdiyana, Sri Anggraeni, Wafa Raihana Arwa, and Abdulkareem Sh Mahdi Al-Obaidi. "Synthesis of carbon microparticles from red dragon fruit (Hylocereus undatus) peel waste and their adsorption isotherm characteristics." *Molekul* 15, no. 3 (2020): 199-209.. http://dx.doi.org/10.20884/1.jm.2020.15.3.657

[36] Nayak, Amit Kumar, and Dilipkumar Pal. "Tamarind seed polysaccharide: an emerging excipient for pharmaceutical use." *Indian J Pharm Educ Res* 51 (2017): S136-46. https://doi.org/10.5530/ijper.51.2s.60

[37] Yaashikaa, P. R., P. Senthil Kumara, Sunita Varjani, and A Saravanan. "A critical review on the biochar production techniques, characterization, stability and applications for circular bioeconomy." *Biotechnology Reports 28*, (2020): e00570. https://doi.org/10.1016/j.btre.2020.e00570

[38] Ragadhita, Risti, and Asep Bayu Dani Nandiyanto. "How to calculate adsorption isotherms of particles using two-parameter monolayer adsorption models and equations." *Indonesian Journal of Science and Technology* 6, no. 1 (2021): 205-234. https://doi.org/10.17509/ijost.v6i1.32354

[39] Pratiwi, Restiani Alia, and Asep Bayu Dani Nandiyanto. "How to read and interpret UV-VIS spectrophotometric results in determining the structure of chemical compounds." *Indonesian Journal of Educational Research and Technology* 2, no. 1 (2021): 1-20. https://doi.org/10.17509/ijert.v2i1.35171

[40] Nandiyanto, Asep Bayu Dani, Risti Ragadhita, Rosi Oktiani, Ajeng. Sukmafitri, and Meli Fiandini. "Crystallite sizes on the photocatalytic performance of submicron WO3 particles." *Journal of Engineering Science and Technology* 15, no. 3 (2020): 1506-1519.

[41] Nandiyanto, Asep Bayu Dani, Rosi Oktiani, and Risti Ragadhita. "How to read and interpret FTIR spectroscope of organic material." *Indonesian Journal of Science and Technology 4,* no. 1 (2019): 97-118. https://doi.org/10.17509/ijost.v4i1.15806

[42] Nandiyanto, Asep Bayu Dani, Risti Ragadhita R, and Meli Fiandini. "Interpretation of Fourier transform infrared spectra (FTIR): A practical approach in the polymer/plastic thermal decomposition." *Indonesian Journal of Science and Technology* 8*,* no. 1 (2023): 113-126. https://doi.org/10.17509/ijost.v8i1.53297

[43] Sukamto, S, and Ali Rahmat. (2023). "Evaluation of FTIR, macro and micronutrients of compost from black soldier fly residual: In context of its use as fertilizer." *ASEAN Journal of Science and Engineering* 3, no. 1: 21-30. https://doi.org/10.17509/ajse.v3i1.42798

[44] Obinna, E.N. "Physicochemical properties of human hair using Fourier Transform Infra-Red (FTIR) and Scanning Electron Microscope (SEM)." *ASEAN Journal for Science and Engineering in Materials* 1, no, 2 (2022): 71-74.

[45] Geng, Yani, Jun Zhang, Jinhong Zhou, and Ji Lei. "Study on adsorption of methylene blue by a novel composite material of TiO 2 and alum sludge." *RSC advances* 8, no. 57 (2018): 32799-32807. https://doi.org/10.1039/C8RA05946B

[46] Gorzin, Fatemeh, and M. M. Bahri Rasht Abadi. "Adsorption of Cr (VI) from aqueous solution by adsorbent prepared from paper mill sludge: Kinetics and thermodynamics studies." *Adsorption Science & Technology* 36, no. 1-2 (2018): 149-169. https://doi.org/10.1177/0263617416686976

[47] Radnia, Hamideh, Ali Asghar Ghoreyshi, Habibollah Younesi, and Ghasem D. Najafpour. "Adsorption of Fe (II) ions from aqueous phase by chitosan adsorbent: equilibrium, kinetic, and thermodynamic studies." *Desalination and Water Treatment* 50, no. 1-3 (2012): 348-359. https://doi.org/10.1080/19443994.2012.720112